

Numerical Analysis of 1×4 Photonic Crystal Fiber Multiplexer

Assia Ahlem Harrat¹, Mohammed Debbal^{1, 2, *},
and Mohammed Chamse Eddine Ouadah^{2, 3}

Abstract—A brand-new four-channel mux system built entirely out of multicore photonic crystal fiber (PCF) structures, which permit wavelength multiplexing at 0.85, 1.19, 1.1, and 1.35 μm , has been confirmed. The multiplexer is a device that sends multiple messages or signals simultaneously via one communication channel. PCF is a category of optical fiber primarily according to the characteristics of photonic crystals, and it is an effective waveguide based on the interaction of microstructured materials with various refractive indices. Silica substance was used to fill up a few air-hole places to optimize the PCF mux structure along with coupling light between more nearby ports (cores) over the PCF axis. The low-index portions are air holes that may be found anywhere along the length of the fiber, and the background material is often natural silica.

1. INTRODUCTION

Effective waveguide known as photonic crystal fiber (PCF) is founded on the microstructural fusion of materials with various refractive indices [1–3]. The low-index portions are air holes that may be positioned throughout the length of the fiber, and the background material is typically natural silica. The extraordinary potential of employing PCF design in contrast to traditional fibers has been supported by numerous publications [4–9]. The ability to incorporate special substances with a wide range of refractive index values is the primary advantage of building a mux device using a PCF design. This is because the bandgap [10, 11] and modified total internal reflection (MTIR) [12, 13] are the basis of light-guiding mechanisms in PCF. The ability to reduce coupling length is the other gain, particularly compared to tightly coupled ports (cores).

A core defect zone has air holes evenly distributed around it in the cladding area to produce PCFs. Figure 1 shows the geometrical features of the PCF structure; d stands for the diameter of the air hole; and Λ (Pitch) is the space between two air holes. Typically, pure silica serves as the background material, and air holes are spaced evenly over the length of the fiber to create lower-index areas. Table 1 shows the parameter value of the structure, and Table 2 shows the index of refraction values of the materials for the chosen wavelength (0.85, 1.1, 1.19, 1.35 μm).

Multiplexers produce a single output signal by combining many input signals (sources) sent by distinct wavelengths. Many benefits of multiplexing include the ability to send numerous signals at once and minimal bit errors with a lot of data bitrate on a single channel [14].

Figure 2 illustrates a multiplexer device, a sophisticated electronic component capable of efficiently combining and transmitting multiple signals from various sources (N input signals) over a single communication line, resulting in a unified output signal. This innovative technology plays a crucial role in streamlining data transmission processes by allowing the convergence of diverse information streams into a compact and manageable form, significantly enhancing the overall efficiency and effectiveness of communication systems.

Received 27 April 2023, Accepted 9 August 2023, Scheduled 23 August 2023

* Corresponding author: Mohammed Debbal (debbal.mohammed@gmail.com).

¹ Belhadj BOUCHAIB University, Ain-Temouchent, Algeria. ² Telecommunications Laboratory of Tlemcen (LTT), Tlemcen 13000, Algeria. ³ Department of Telecommunications, Faculty of Electrical and Computer Engineering, Mouloud MAMMERI University, Tizi-Ouzou 15000, Algeria.

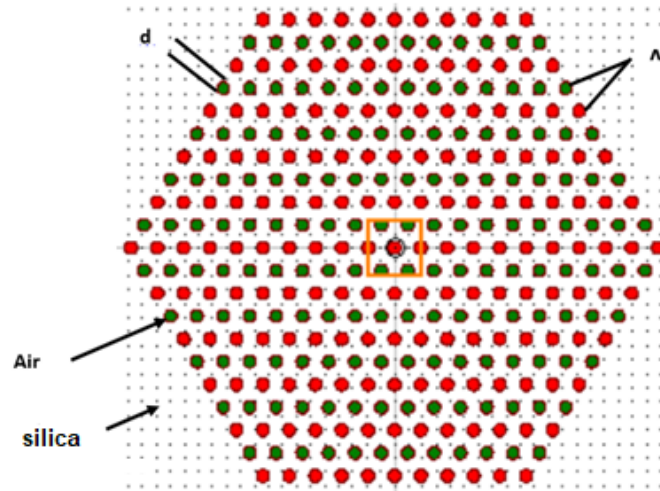


Figure 1. Photonic crystal fiber structure.

Table 1. The parameter of the PCF.

<i>Parameter</i>	<i>Value</i>
Pitch (Λ)	1.88 (μm)
Diameter (d)	0.9 (μm)
Length of fiber (Z)	6000 (μm)
n_{air}	1

Table 2. The refractive index of silica of the four selected wavelength.

λ (μm)	0.85	1.1	1.19	1.35
n_{silica}	1.4525	1.4492	1.44816	1.44635

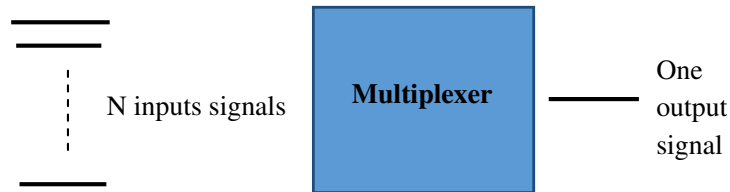


Figure 2. Example of multiplexer device.

There have been reports of many mux based on photonic crystal fiber. They have suggested using an oil-filled photonic crystal fiber with four-wave mixing (FWM) to create a fiber temperature sensor (PCF) and employing innovative hexagonal mid-gapped tiered PCF mode group equalizers and three-core photonic crystal fiber (PCF) mode group multiplexers that benefit from optical space division multiplexing to improve the signal quality and increase the range of the connection in a rural setting, and for the first time, a CirD laser for wavelength division multiplexing (WDM) applications is produced using the finite-difference time-domain approach in three dimensions [15–19].

Several methods, employing various air-hole sizes in the PCF structure and altering the PCF index

profile by replacing some air-hole regions with pure silica over the fiber length [20–22], have been used to demonstrate the ability to link light between nearby ports (cores) in a PCF construction.

This study showed how a PCF structure can split four wavelengths into a 1×4 wavelength mux. The working range of wavelengths is 0.85, 1.1, 1.19, and 1.35 μm . Over the length of the fiber, some areas with air holes were replaced with natural silica material to achieve the light coupling between the tighter linked cores.

As far as we can tell, this paper aims to look at how silica integrated across a multicore PCF structure can be utilized to influence the direction of light propagation. The results of this research were used to develop a unique multiplexer that worked throughout the multicore PCF structure with no additional optical components needed. An innovative technique to reduce the cost and dimensions of the optical communication system might be developed as a result of this.

2. MATERIALS AND METHODS

Respectively, on the XZ plane ($y = 0 \text{ mm}$), XY plane ($z = 0 \text{ mm}$), and XY plane ($z = 6 \text{ mm}$), Figures 3(a)–(c) depict the entire mux PCF design refractive index profile structure. In these figures, the natural silica background material is indicated in a red tint, while the air-hole regions are highlighted

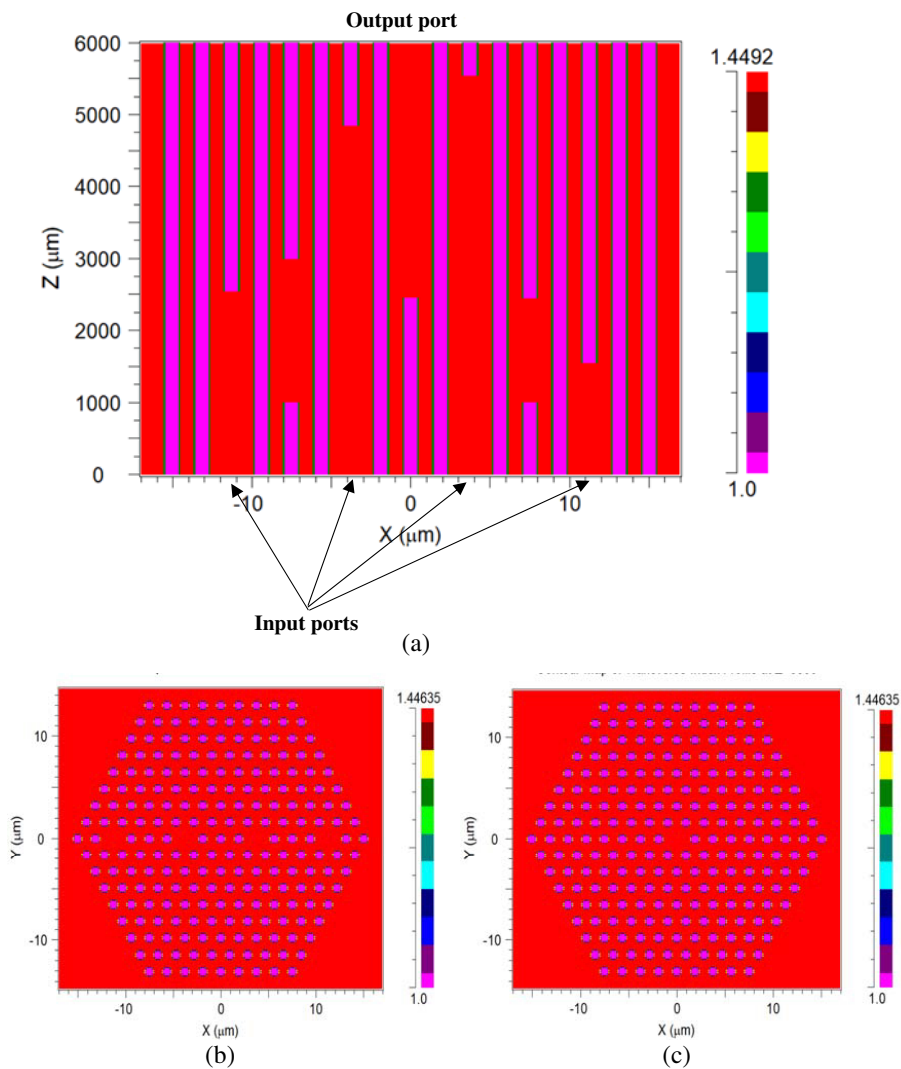


Figure 3. Refractive index profile of the 1×4 wavelength mux: (a) XZ plane at $y = 0 \text{ mm}$. (b) XY plane at $z = 0 \text{ mm}$. (c) XY plane at $z = 6 \text{ mm}$.

in purple, and d , Λ (pitch), and z are the geometrical characteristics of the PCF design.

The main functionality of the PCF mux device is based on regulating the light coupling length size between two nearby ports and confining light inside the channel (core). A pure silica high-index material along the length of the fiber can be used to replace some air-hole actors to achieve these effects.

Since the modified total internal reflection (MTIR) serves as the foundation for the light-guiding mechanism in our concept, light can be linked between two closer ports with the same index of refraction value, and a port with a high index value can accomplish significant light confinement (pure silica).

The four input ports (ports 1, 2, 3, and 4) at $z = 0$ and one output port at $z = 6$ mm are shown in Figures 3(b) and (c).

3. RESULTS

The input/output beam of the four wavelengths 0.85, 1.1, 1.19, and 1.35 μm at the x - y plane is depicted in Figures 4 and 5. After a distance of 6 mm, we observed that our input signals were merged into just one output port, indicating that the power multiplexer had an impact.

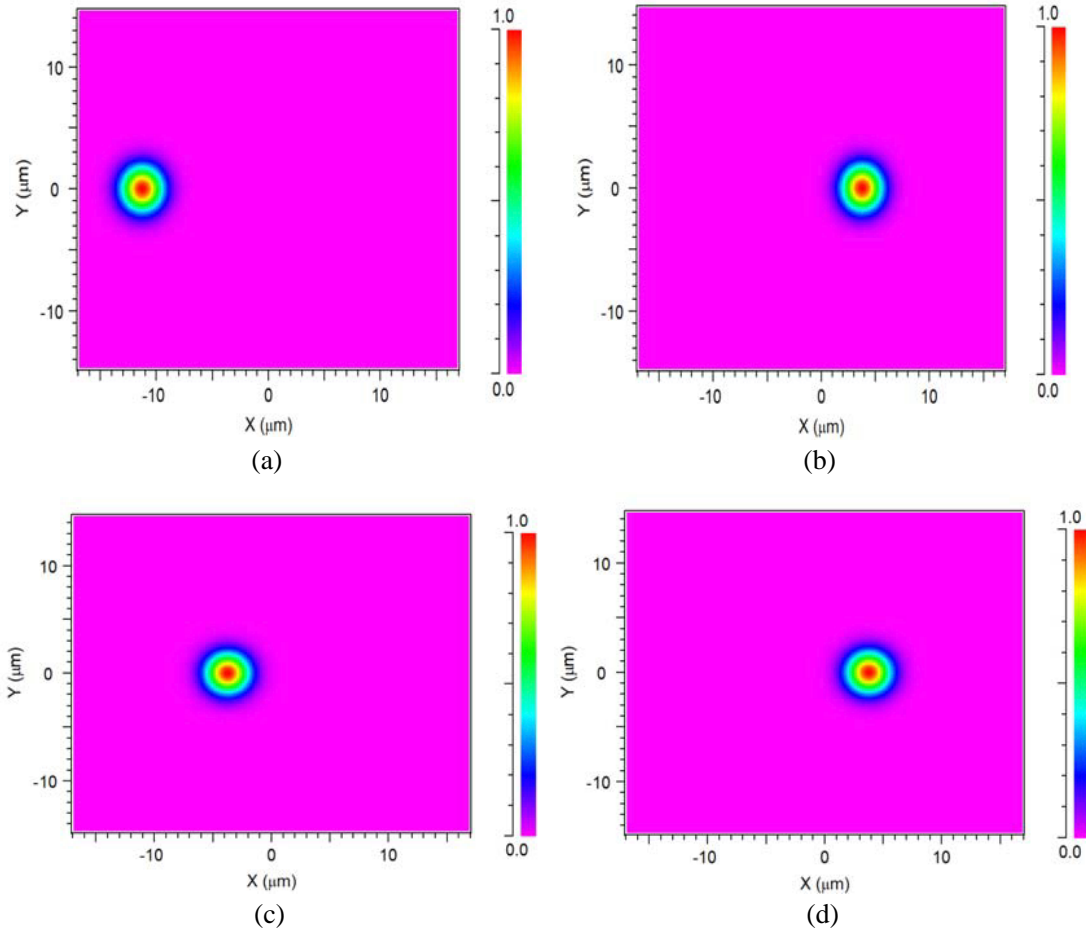


Figure 4. The 1×4 input power multiplexing of the four optical signals (a) $\lambda = 0.85 \mu\text{m}$; (b) $\lambda = 1.1 \mu\text{m}$; (c) $\lambda = 1.19 \mu\text{m}$; (d) $\lambda = 1.35 \mu\text{m}$ at $z = 0$ mm.

Figure 6 demonstrates the light coupling between cores and the light propagating over the entire fiber length at the x - z plane for the selected wavelength channels.

Figure 6(a) depicts the optical path from the beginning of the transmission ($\lambda_1 = 0.85 \mu\text{m}$) to the center (the output), passing through the various stages: from input channel 1, which represents port 1,

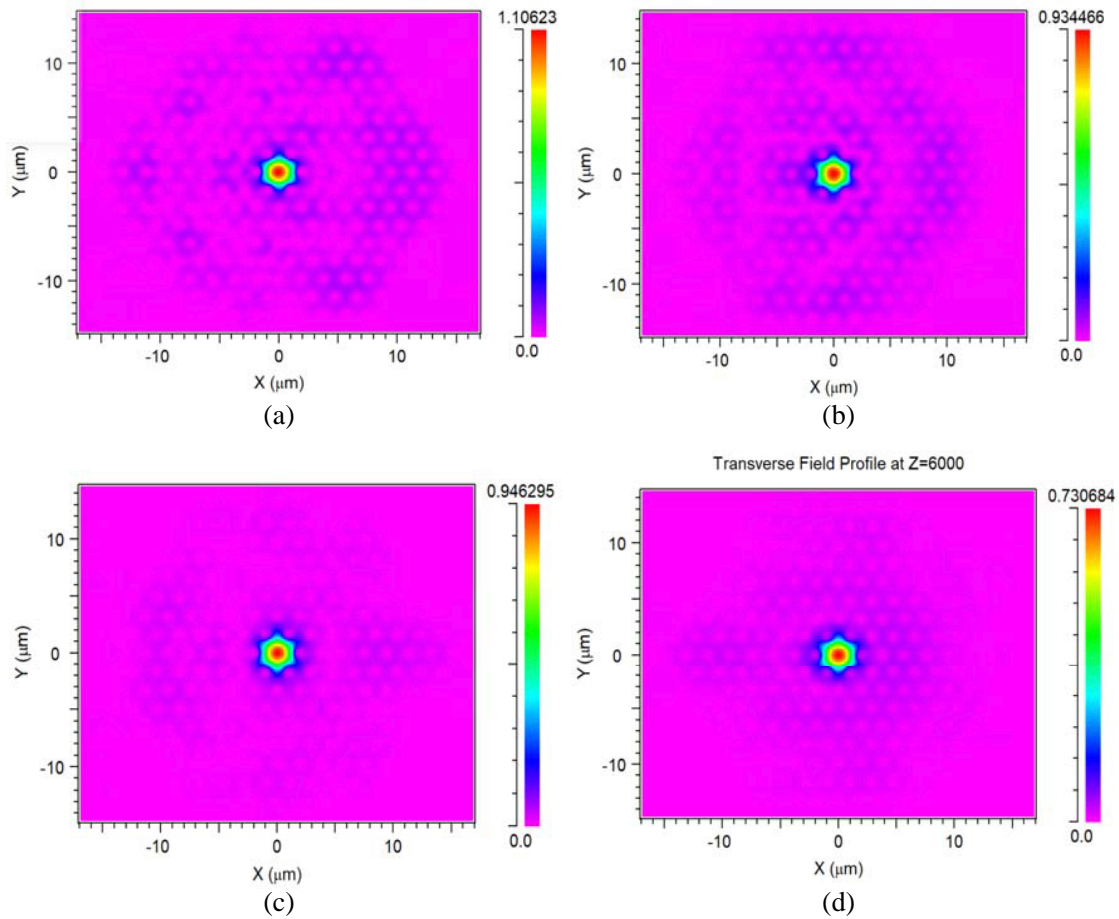


Figure 5. The 1×4 input power multiplexing of the four optical signals (a) $\lambda = 0.85 \mu\text{m}$; (b) $\lambda = 1.1 \mu\text{m}$; (c) $\lambda = 1.19 \mu\text{m}$; (d) $\lambda = 1.35 \mu\text{m}$ at $z = 6 \text{ mm}$.

to the output channel (port 4), by coupling between the two closed ports 1 and 2 at $z = 2.5 \text{ mm}$; the second z step occurs at $z = 2.9 \text{ mm}$ where the light is directed to the output channel (from port 2 to port 3); the third z step occurs at 4 mm from port 3 to 4 then at 4.2 from port 4 to 5. When $z = 5.5 \text{ mm}$, the light is finally constrained inside the core region and propagates the output channel.

The optical path from input channel 2: $\lambda_2 = 1.1 \mu\text{m}$ (representing port 5) to the output channel (port 4) is depicted in Figure 6(b), by coupling between the two closed ports 5 and 6 at $z = 1.6 \text{ mm}$; the second z step occurs at $z = 2.45 \text{ mm}$ where the light is directed to the output channel (from port 6 to port 5); the third z step occurs at 3.2 from port 5 to 4 then at 3.4 mm from 4 to 3 and from 3 to 5 at 4.3 mm . After being finally restricted inside the core region at $z = 5.35 \text{ mm}$, the light propagates from port 5 to the output channel.

The optical path from the beginning of transmission ($\lambda_3 = 1.19 \mu\text{m}$) to the center (the output) is depicted in Figure 6(c), passing through several stages: from input channel 3, which corresponds port 3, to the output channel (port 4), by coupling between the two ports 3 and 1, passing by port 2 at $z = 1.4 \text{ mm}$; the second z step occurs at $z = 2.55 \text{ mm}$ where the light is directed to the output channel (from port 1 to port 3 passing by different steps); the third z step occurs at 4.85 mm from port 3 to 5 passing by port 4. The light is eventually contained inside the core region at $z = 5.55 \text{ mm}$, where it propagates from port 5 to the output port 4.

The optical path from the beginning of transmission ($\lambda_4 = 1.35 \mu\text{m}$) to the center (the output) is depicted in Figure 6(d), passing through several stages: from input channel 4, which corresponds to port 7, to the output channel (port 4), by coupling between the two ports 7 and 5, passing by port 6 at $z = 1.4 \text{ mm}$; the second z step occurs at $z = 2.8 \text{ mm}$ where the light is directed to the output channel

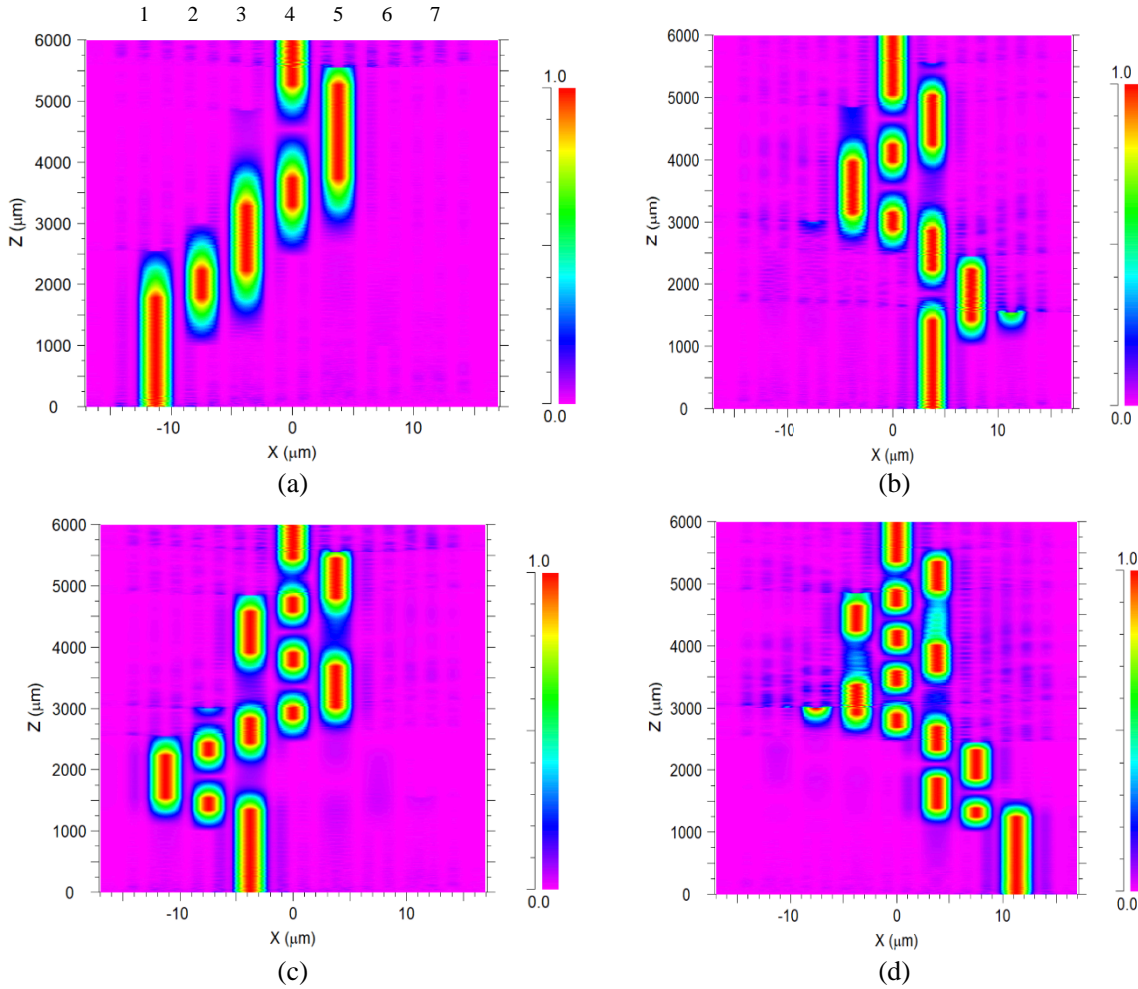


Figure 6. Profile of intensity of the 1×4 wavelength multiplexer. (a) for the optical signal $\lambda = 0.85 \mu\text{m}$; (b) $\lambda = 1.1 \mu\text{m}$; (c) $\lambda = 1.19 \mu\text{m}$; (d) $\lambda = 1.351 \mu\text{m}$.

(from port 5 to port 3 passing by different steps and the third z step at 4.85 mm from port 3 to port 5. The light propagates from port 5 to output port 4 before being eventually trapped inside the core region at $z = 5.55$ mm.

Figures 7(a)–(b) show that the input power in the core reaches a maximum of 81% before falling to zero at 1.02 mm, so that the input power, which must pass through numerous stages as it moves from one segment to its neighbor with light coupling, can be concentrated on the output port. At 2.48 mm and 2.493 mm for Figures 7(a) and (b), respectively, the output port power starts to rise and reaches a maximum of 54%.

Up to a distance of 1.26 mm, the beginning power of the transmission is 80%, and we saw transmission losses of 20% as a result of the absorption of intrinsic materials, bends, and connection loss. Beyond this point, though, the signal in the input segment will be zero because it is now pointed to the output port. We placed a silica hole at various phases to produce a coupling zone and magnify our signal. The power increases at the output port from 0% to 45.6% after traversing 6 mm (Figure 7(c)).

We see in Figure 7(d) that the input power in the core is at a high of 83% and then decreases to zero at 1.01 mm. This is because the input power will be focused on the output port after traveling through several stages from one segment to its adjacent segment with light coupling. The output port power begins to increase at 2.47 mm and increases to a maximum of 33%.

Signal transmission at $z = 0$ mm and $z = 6$ mm is shown in Figures 8 and 9(a)–(d). Figure 8 shows our four optical signals at their initial maximum (100%). Nonetheless, high transmission of 100% for the core ($0.85 \mu\text{m}$), 94% for the core ($1.1 \mu\text{m}$), 93% for the core ($1.19 \mu\text{m}$), and 73% for the core ($1.35 \mu\text{m}$)

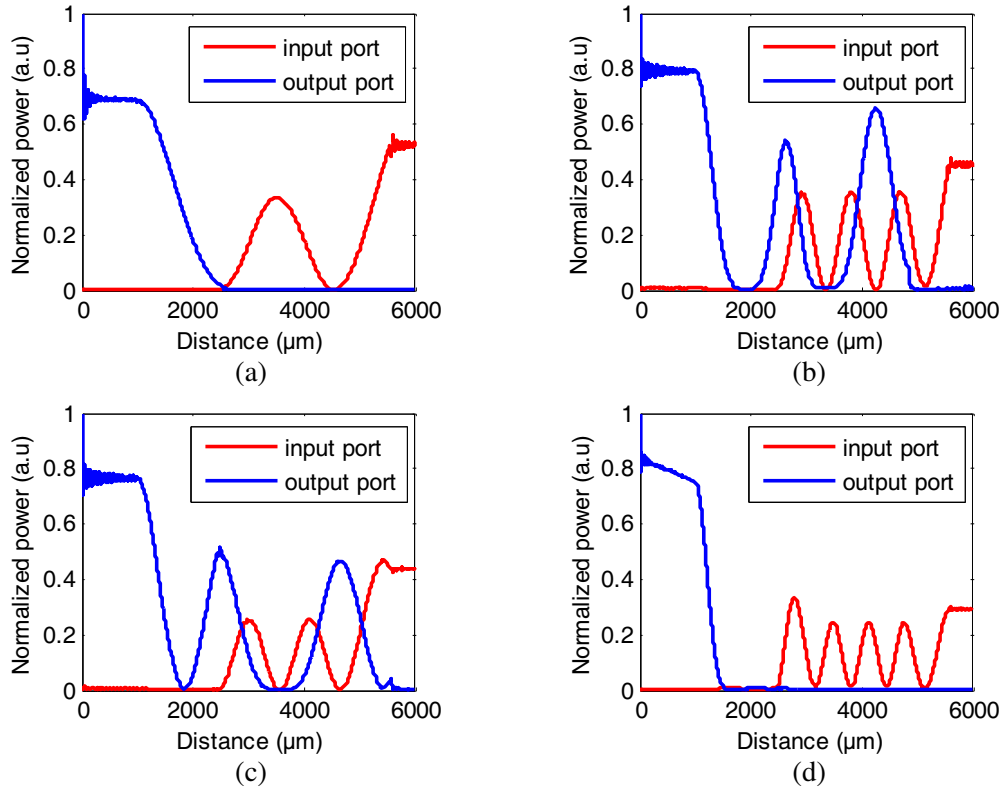


Figure 7. Standardized input and output power of $1 * 4$ power multiplexer for the optical signals $\lambda_1 = 0.85 \mu\text{m}$, $\lambda_2 = 1.1 \mu\text{m}$, $\lambda_3 = 1.19 \mu\text{m}$, and $\lambda_4 = 1.35 \mu\text{m}$.

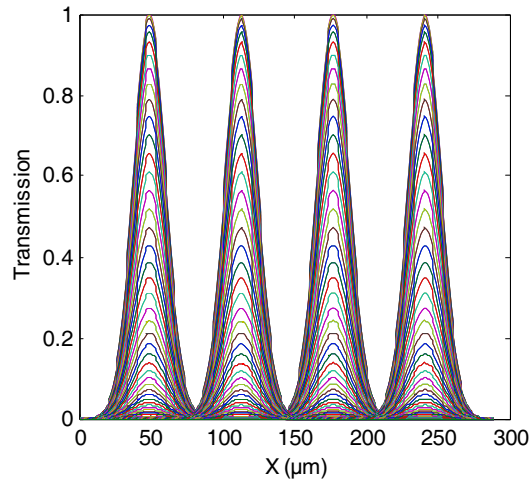


Figure 8. The normalized coupling efficiency at $z = 0 \text{ mm}$.

was reached, which is a good result. This was made possible by combining the signals into one port at the output (6 mm).

In this study, we have employed the Beam Propagation method, along with specific Opto-geometric parameters ($d = 0.9$ and $\Lambda = 1.88 \mu\text{m}$), with the primary objective of enhancing the performance of our optical structure. We aimed to improve the transmission efficiency through our device and compare our findings with the results obtained in a previous study conducted by Gelkop et al., which also utilized the Beam Propagation method but with different parameters [22].

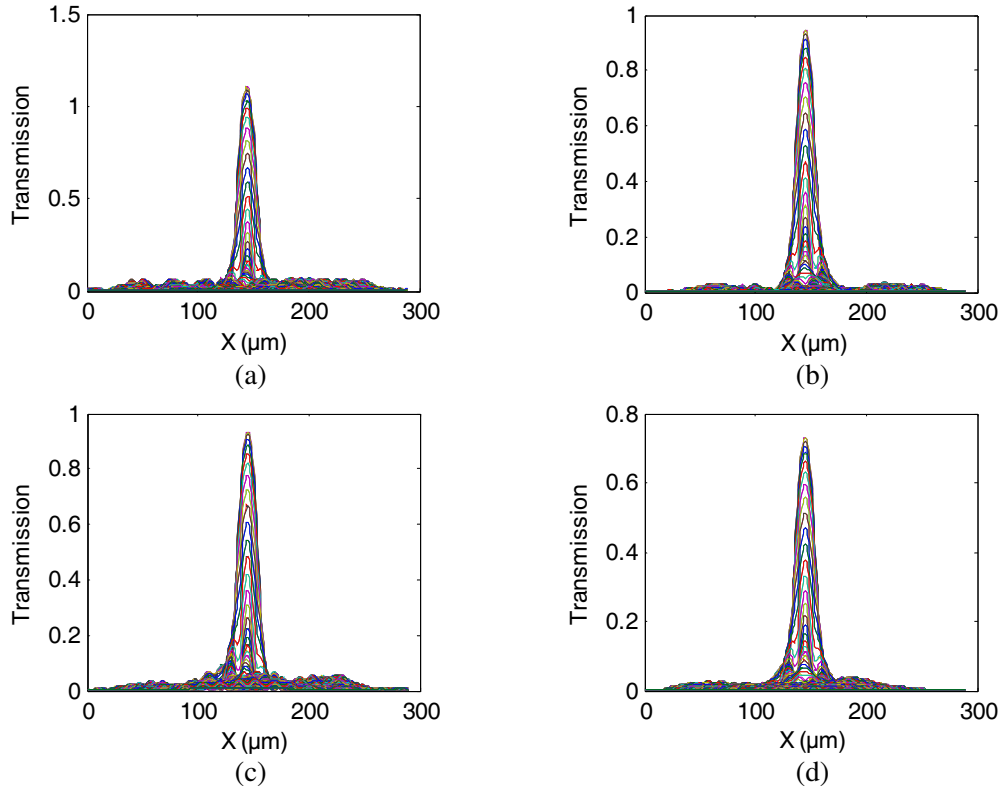


Figure 9. The normalized coupling efficiency at $z = 6$ mm for the (a) $0.85 \mu\text{m}$, (b) $1.1 \mu\text{m}$, (c) $1.19 \mu\text{m}$, (d) $1.35 \mu\text{m}$.

After conducting our experiments and analyses, we have achieved remarkable results in terms of transmission efficiency. Specifically, we obtained transmission rates of 100% for channel-1, 94% for channel-2, 93% for channel-3, and 73% for channel-4. These outcomes demonstrate a significant improvement compared to the reference study, which reported transmission rates of 88% for channel-1, 80% for channel-2, and 79% for channel-3.

The notable improvement in our transmission efficiency can be attributed to the utilization of the specific Opto-geometric parameters, namely $d = 0.9$ and $\Lambda = 1.88 \mu\text{m}$, which proved to be better suited for optimizing light transmission in our experimental setup.

These findings hold promising implications for various applications, such as optical communications and information processing systems, where efficient light transmission is crucial. Our work highlights the potential benefits of employing the Beam Propagation method with these particular Opto-geometric parameters.

Further investigations and experiments could be pursued in the future to explore the full potential and limitations of these parameters and to further improve the overall performance of our optical structure. This may lead to advancements in the field of photonics and optical device design, enhancing the capabilities of various optical systems in practical applications.

4. CONCLUSION

This work shows how the MTIR mechanism may be used for controlling the direction of light propagation within the multicore PCF, allowing light to couple the silica parts solely, and achieve more light confinement for the higher index material.

The simulation results demonstrated that after a propagation length of 6 mm, the operating wavelengths of $0.85 \mu\text{m}$, $1.1 \mu\text{m}$, $1.19 \mu\text{m}$, and $1.35 \mu\text{m}$ could be built.

According to simulation results, the four wavelengths can propagate through the device and be multiplexed with the best outcomes. Transmission is 73, 93, 94, and 100% for the output port 1.35, 1.19, 1.1, and 0.85 μm wavelength after a distance of 6 mm.

This study can be utilized by using multicore photonic crystal fiber as the basis for a revolutionary and powerful multiplexer device in the future if the appropriate modifications are made to the materials.

With the directed light traveling in the opposite direction, the multiplexer can also function as a demultiplexer. The simulation outcomes confirmed that after a 6 mm light propagation, the four-channel mux can start to demultiplex. Consequently, the suggested technology can be used in the future to improve networking structure performance.

REFERENCES

1. De, M., T. K. Gangopadhyay, and V. K. Singh, "Prospects of photonic crystal fiber as physical sensor: An overview," *Sensors*, Vol. 19, No. 3, 464, 2019.
2. Knight, J., T. Birks, P. S. J. Russell, and J. De Sandro, "Properties of photonic crystal fiber and the effective index model," *JOSA A*, Vol. 15, No. 3, 748–752, 1998.
3. Van, L. C., K. D. Xuan, T. Le Canh, T. T. Doan, T. N. Thi, and H. Van Le, "Supercontinuum generation in chalcogenide photonic crystal fiber infiltrated with liquid," *Optical Materials*, Vol. 137, 113547, 2023.
4. Liu, Y., et al., "Highly sensitive temperature sensor based on Sagnac interferometer using photonic crystal fiber with circular layout," *Sensors and Actuators A: Physical*, Vol. 314, 112236, 2020.
5. Du, H., X. Sun, Y. Hu, X. Dong, and J. Zhou, "High sensitive refractive index sensor based on cladding etched photonic crystal fiber Mach-Zehnder interferometer," *Photonic Sensors*, Vol. 9, 126–134, 2019.
6. Butt, M., S. N. Khonina, and N. Kazanskiy, "Recent advances in photonic crystal optical devices: A review," *Optics & Laser Technology*, Vol. 142, 107265, 2021.
7. Kumar, D., M. Khurana, M. Sharma, and V. Singh, "Analogy of gold, silver, copper and aluminium based ultra-sensitive surface plasmon resonance photonic crystal fiber biosensors," *Materials Today: Proceedings*, 2023.
8. Guo, Z., J. Yuan, C. Yu, X. Sang, K. Wang, B. Yan, L. Li, S. Kang, and X. Kang, "Highly coherent supercontinuum generation in the normal dispersion liquid-core photonic crystal fiber," *Progress In Electromagnetics Research M*, Vol. 48, 67–76, 2016.
9. Ouadah, M. C. E., M. Debbal, H. Chikh-Bled, and M. Bouregaa, "Effect of the temperature and the geometrical parameters on the modal properties of circular photonic crystal fiber," *Progress In Electromagnetics Research M*, Vol. 115, 1–10, 2022.
10. Li, W., T. Matniyaz, S. Gafsi, et al., "151 W monolithic diffraction-limited Yb-doped photonic bandgap fiber laser at ~ 978 nm," *Optics Express*, Vol. 27, No. 18, 24972–24977, 2019.
11. Gangwar, R. K., A. K. Pathak, J. Qin, and X. Wang, "Physics of photonic crystals and applications," *Modern Luminescence from Fundamental Concepts to Materials and Applications*, 313–327, Elsevier, 2023.
12. Li, M., R. Singh, M. S. Soares, C. Marques, B. Zhang, and S. Kumar, "Convex fiber-tapered seven core fiber-convex fiber (CTC) structure-based biosensor for creatinine detection in aquaculture," *Optics Express*, Vol. 30, No. 8, 13898–13914, 2022.
13. Kiroriwal, M. and P. Singal, "Broadband mid-infrared supercontinuum generation in AlGaAs photonic crystal fibers by liquid infiltration and rod-filling approaches," *Journal of Computational Electronics*, 1–8, 2023.
14. Parandin, F. and A. Sheykhanian, "Design and simulation of a 2×1 all-optical multiplexer based on photonic crystals," *Optics & Laser Technology*, Vol. 151, 108021, 2022.
15. Kumar, C. and G. Kumar, "Performance evaluation of OADM for super dense wavelength division multiplexing system," *Progress In Electromagnetics Research Letters*, Vol. 85, 131–135, 2019.

16. Geng, Y., L. Wang, Y. Xu, A. Kumar, X. Tan, and X. Li, "Wavelength multiplexing of four-wave mixing based fiber temperature sensor with oil-filled photonic crystal fiber," *Optics Express*, Vol. 26, No. 21, 27907–27916, 2018.
17. Amphawan, A., S. Chaudhary, T.-K. Neo, M. Kakavand, and M. Dabbagh, "Radio-over-free space optical space division multiplexing system using 3-core photonic crystal fiber mode group multiplexers," *Wireless Networks*, Vol. 27, No. 1, 211–225, 2021.
18. Xiong, Y., T. Umeda, X. Zhang, et al., "Photonic crystal circular-defect microcavity laser designed for wavelength division multiplexing," *IEEE Journal of Selected Topics in Quantum Electronics*, Vol. 24, No. 6, 1–7, 2018.
19. Priyadharshini, C., R. Devika, S. Selvendran, and A. S. Raja, "Investigating the cross core octagonal photonic crystal fiber with high birefringence: A design and analysis study," *Materials Today: Proceedings*, 2023.
20. Malka, D. and G. Katz, "An eight-channel C-band demux based on multicore photonic crystal fiber," *Nanomaterials*, Vol. 8, No. 10, 845, 2018.
21. Dadabayev, R. and D. Malka, "A visible light RGB wavelength demultiplexer based on polycarbonate multicore polymer optical fiber," *Optics & Laser Technology*, Vol. 116, 239–245, 2019.
22. Gelkop, B., L. Aichnboim, and D. Malka, "RGB wavelength multiplexer based on polycarbonate multicore polymer optical fiber," *Optical Fiber Technology*, Vol. 61, 102441, 2021.